Journal of Applied Polymer Science

Optimization of Amphiphobic Structural Surface Thickness in Relation to its Functionality on Stainless Steel Plates

Wei-Li Yuan,[1] Chi-Jung Su,[2] Chien-Ming Lei,[3] Chun-Yueh Mou[1]

[1]Department of Chemical Engineering, Feng Chia University, Taichung 40724, Taiwan, Republic of China
[2]School of Medical Applied Chemistry, Chung Shan Medical University, Taichung 40201, Taiwan, Republic of China
[3]Department of Chemical and Materials Engineering and Graduate Institute of Nanomaterials, Chinese Culture University, Taipei 11114, Taiwan, Republic of China
Correspondence to: C.-Y. Mou (E-mail: cymou165@gmail.com)

ABSTRACT: Fluorine-based amphiphobic coatings have been widely used in commercial textiles to provide water- and oil-repelling abilities. However, few reports from the literature survey have discussed the surface structural effects of the coated substrate on amphiphobicity. In this research, various thickness amphiphobic coatings based on mixed epoxy, tetraethylorthosilicate, and a particular alkoxysilane with fluorinated side chains (F-silane) were deposited on Grade 420 stainless steel plates. Film amphiphobicity is characterized by measuring the water and oil contact angles of the coating. Film morphology is examined using atomic force microscopy. The deposited films free of F-silane are thinner than 150 nm. The films become thick at high F-silane volume percentage with the surface cavities, ridges, and granules being masked out. On the addition of F-silane, the water contact angle of the deposited films increases up to 105° and then reaches a plateau of ~ 107° with increasing F-silane. In contrast, the oil contact angle increases up to 60° at first and then slowly declines with the F-silane concentration. The total drop of oil contact angle by ~ 20° was attributed to the masking out of surface features on film thickening. This indicates that the surface oleophobicity depends on surface structures. Therefore, improving surface amphiphobicity correlates with creating more refined multiscale surface structures during the industrial manufacturing process of steel plate, prior to surface modification by F-silane. © 2014 Wiley Periodicals, Inc. J. Appl. Polym. Sci. **2014**, *131*, 41003.

KEYWORDS: applications; coatings; microscopy; morphology

Received 16 February 2014; accepted 12 May 2014
DOI: 10.1002/app.41003

INTRODUCTION

Through the history of evolution, many biological materials, such as lotus leaves, rice leaves, butterfly wings, mosquito compound eyes, cicada wings, rose petals, and spider silks, exhibit surface superhydrophobicity.[1–7] These products of nature have been the source of inspiration to many scientists and engineers who try to use the interactions between the fine hierarchical structures of solids and the fluids in contact to control the surface wettability. Special wetting phenomena include superhydrophobicity,[8,9] superhydrophilicity,[10,11] superoleophobicity,[12,13] and superoleophilicity.[14,15] Materials combining any of the four wetting behaviors just mentioned might find interesting and profitable applications for the industry. For example, superhydrophobic and superoleophobic surfaces (also known as superamphiphobic surfaces) of textiles exhibit self-cleaning properties by repelling water and oil spilled on the surface.[16]

Cassie and Baxter[17] and Wenzel[18] proposed that a solid surface can be microscopically roughened to increase its original hydrophobicity. The Cassie model describes a wetted state of a superhydrophobic surface with water droplets deposited above the surface textures rather than in between them.[17] Later on, it was discovered that the height and width of the textures, as well as the distance between them, are critical in achieving the Cassie state.[19]

Artificial superhydrophobic surfaces have been developed over the years to serve us daily in industry, environment, and biomedicine. For example, several techniques have been developed to roughen a plane surface, including (1) argon plasma etching of a spin-coated monomer layer to give micro/nanopapillae on polymerization,[20] (2) pyrolysis of metal phthalocyanines to form aligned carbon nanotube film,[21] (3) using two polymers with different solubilities to form micro/nanohierarchical papillae,[22] (4) electrochemical deposition of microscale and nanoscale hierarchical structured copper mesh films,[23] (5) electrochemical deposition of variously shaped gold nanostructures,[24] (6) using a layer of self-assembled polymer

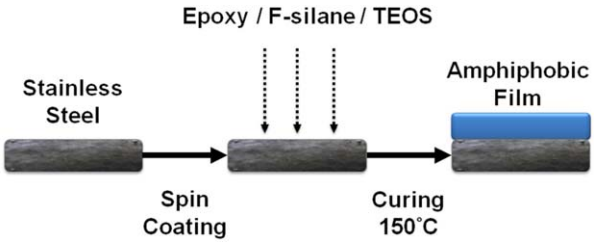

Figure 1. Process for depositing amphiphobic coatings on silicon wafers. The coating formula comprises epoxy resin as film matrix, crosslinker for curing, F-silane for amphiphobicity, and TEOS for film hardening. [Color figure can be viewed in the online issue, which is available at wileyonlinelibrary.com.]

microspheres to create a hierarchical bowl-like array of silver particles bonded with alkanethiol to lend superhydrophobicity,[25–27] and (7) deposition of highly fluorinated, random, ribbon-shaped, and micrometer-long structures on polyethyleneterephthalate substrates by plasma-enhanced chemical vapor deposition for experiments on cell adhesion, growth, and proliferation.[28]

Furthermore, superhydrophobicity often goes together with superoleophobicity to produce water- and oil-repelling materials. On one hand, amphiphobic materials containing fluoroalkyl segments or branches such as Teflon and poly(vinylidene fluoride) have been widely studied and used. Their innate water-/oil-repelling properties arise from the small radius and high electron affinity of fluorine atom.[29,30] On the other hand, new and innovative ways to give materials effective amphiphobic coating have been published throughout the last decade. For example, scientists have found that extremely superamphiphobic surface can be produced based on fluorinated silica nanoparticles,[31] that flexible, high heat-resistant, and amphiphobic silica nanofibrous mats can be fabricated by (fluoroalkyl)silane electrospinning,[32] and that core–shell–corona particles can be prepared from monomer methyl methacrylate and crosslinker ethylene glycol dimethacrylate to produce a coating that is amphiphobic on glass.[33] Silanes with fluorinated groups or side chains (F-silane) are low in surface tension, water-/oil-repelling, contaminant resistant, and chemically stable.[34–36] However, it is normally less than ideal for the fluorine-containing coatings to adhere strongly enough to metallic substrates.[37] Common methods to raise the bonding between fluorinated coating and metal substrate involve increasing the roughness of the metal by physical or chemical means to enlarge the contact area.

Although there is much advancement in this field of technology, there are many concerns such as cost, process, and vulnerability to environment and humans associated with commercializing the techniques mentioned above.[38] A costly technique for depositing amphiphobic coatings involves using plasma to activate the substrate surface and a reactive vapor of fluorine compound to form a fluorinated surface layer. A more economic way is to apply a buffer layer such as epoxy or glass that provides alkyl or hydroxyl groups to mix or link with F-silane, leading to a stronger coating.

In this study, we seek to identify the most cost-efficient and effective way of making an amphiphobic epoxy coating on stainless steel by determining the minimum yet long-lasting film thickness. To make a long-lasting amphiphobic epoxy coating on stainless steel, silica precursor, F-silane, and epoxy were formulated and mixed in solution before being spread onto the substrates. After film deposition, the sol–gel process[39–41] and epoxy crosslinking were initiated by thermal curing. Surface contact angles of water and oil drops were measured as potency of amphiphobicity. Film morphology was examined using atomic force microscopy (AFM) to understand the geometrical effects of surface features on amphiphobicity. Film thickness was measured using a surface profilometer, and its values were plotted against the amounts of added epoxy for the determination of optimal film thickness.

EXPERIMENTAL

Materials

Diglycidyl ether of bisphenol A (MW = 189; Chang Chun Group, Taiwan) was used as received to form epoxy films. Crosslinker for epoxy (So-5110A) was purchased from Echo-Nanobio, Taiwan. The F-silane with fluorinated side chains (Si-1004L; Echo-Nanobio) was used as amphiphobic agent. Tetraethylorthosilicate (TEOS, 98%; Acros), with formula $Si(OC_2H_5)_4$, was used as received for preparing silica particles in the films. Acetone, 1-butanol, and *n*-hexane (99, 99, and 95%, respectively) were purchased from Acros and used directly as solvent. Stainless steel plates (Grade 420, 5 × 5 cm^2; Jiaxin, Taiwan) were cleaned in ethanol under ultrasonic oscillation for 30 min, rinsed by deionized water, and dried in oven for 30 min before use.

Synthesis and Film Fabrication

A scheme of the amphiphobic film deposition process is shown in Figure 1. Using this method, an amphiphobic epoxy-based coating can be constructed on a stainless steel plate, a silicon wafer, or a glass slide. Film precursor solutions of varied compositions including epoxy, F-silane, and TEOS were prepared and deposited on the substrate by spin coating, with a spin coater (PM490; Pentad Scientific, Taiwan), at 2500 rpm for 20 s. In each deposition, only one drop of the precursor solution (0.02 mL) was used. Deposited films were cured in oven (NTR-800; Grieve) at a temperature 150°C for 10 min. Crosslinked films were rinsed with deionized water and dried in oven at 60°C for 30 min.

Film Analysis

Film thickness was measured using Surfcorder (ET3000; Kosaka Laboratory, Japan). Amphiphobic properties were characterized at room temperature by a contact angle meter (CA-D; Kyowa Interface Science, Japan). Drops of 2-μL water or oil were deposited on the film surface via a syringe, the position of which was adjusted to 0.5 mm above the film surface. Direct measurements of the contact angle were performed at both sides of each drop. During operation, care was taken to keep the drops intact. More than five readings were recorded for each sample, and the average was calculated and reported.[42] Evaluation of surface roughness of the cross-sectional profiles was based on the exported data from the profilometer. The roughness parameter used in this report was the root-mean-square

Table I. Amphiphobic Film Precursor Formulae of Epoxy, F-silane, 1-Butanol, and Acetone

Series	Epoxy (vol %)	F-silane (vol %)	1-Butanol (vol %)	Acetone (vol %)
1 (for Figures 2 and 3)	0.0010	1.5	25.2	25.2
	0.0021	1.5	25.2	25.2
	0.0041	1.5	25.2	25.2
	0.0082	1.5	25.2	25.2
	0.016	1.5	25.2	25.2
	0.041	1.5	25.2	25.2
2 (for Figures 4 and 5)	0.0021	0.0	26.0	26.0
	0.0021	0.2	25.9	25.9
	0.0021	0.7	25.6	25.6
	0.0021	1.5	25.2	25.2
	0.0021	2.9	24.5	24.5
	0.0021	13	19.5	19.5

Note: There are two more ingredients in each recipe, that is, TEOS and *n*-hexane. The compositions of them are both fixed at 24 vol %.

roughness *Rq*, the deviation from the mean height of surface, expressed mathematically as follows:

$$Rq=\sqrt{\int (h(x)-\overline{h})^2 dx/L}, \quad (1)$$

where L is the projection length of the profile on x-axis. The mean height of the surface is calculated as follows:

$$\overline{h}=\int h(x)dx/L, \quad (2)$$

where $h(x)$ is the pixel height or z data collected by AFM.[43]

Surface morphology was examined with a NanoScope IV, multimode SPM from Digital Instruments/Veeco, operated in tapping mode. The cantilevers (spring constant 0.31–0.41 N/m) were purchased from Nanosensors. AFM is a powerful tool to characterize film surface structures on the nanoscopic scale.[44–46]

In coating epoxy films on stainless steel plates, varied volume percentages (vol %) of epoxy in the precursor solution were used to correlate film thickness with epoxy content. A total of 240 mL of mixed epoxy, crosslinking agent, acetone, 1-butanol, F-silane, hexane, and TEOS was prepared, with epoxy varied from 0.0010 to 0.041 vol %. The formulae with main ingredients are shown in Series 1 of Table I. The processed films were analyzed by a profilometer to understand how the thickness changes with epoxy volume percentage.

In Series 2 of Table I, the F-silane volume percentage in the precursor solution was varied to correlate film amphiphobicity with F-silane content. After deposition of films with epoxy fixed at 0.0021 vol % and F-silane altered from 0 to 13 vol %, the contact angles of water and oil on the films were measured.

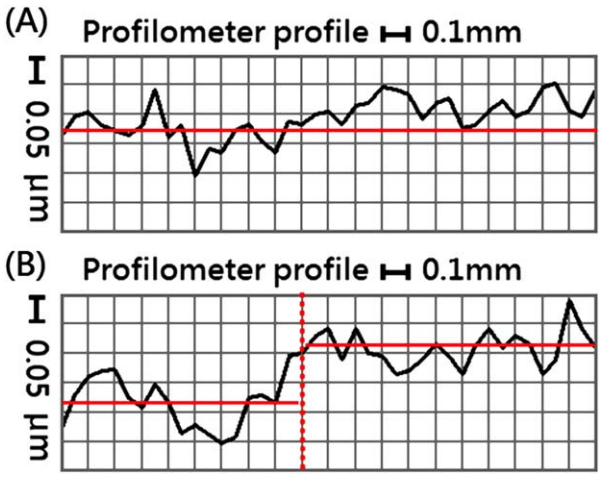

Figure 2. Typical surface profiles of bare (A) and epoxy-coated (B) stainless steel plates. The average film thickness is calculated as the difference between the mean heights of the right profiles and the epoxy film edge as 80 nm. [Color figure can be viewed in the online issue, which is available at wileyonlinelibrary.com.]

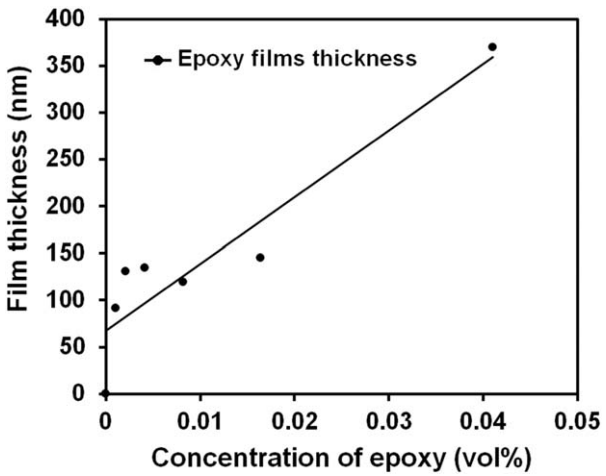

Figure 3. Plot of film thickness against epoxy volume percentage. A straight line was drawn only to show that a larger epoxy volume percentage would result in a thicker film. Films less than 150 nm could be obtained at a low epoxy volume percentage less than 0.01.

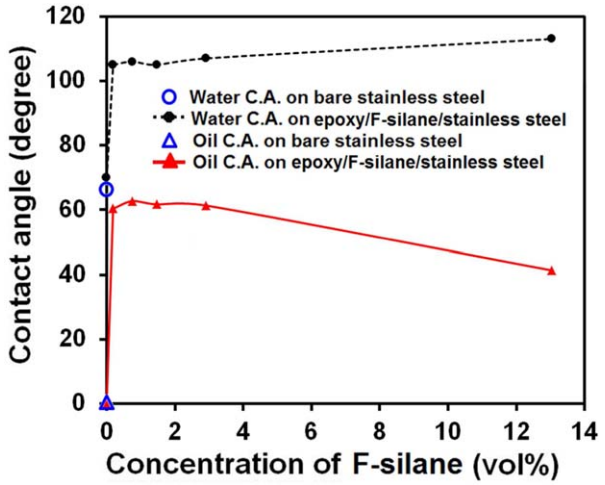

Figure 4. Plot of contact angle against F-silane concentration on epoxy-coated stainless steel plates from solution containing 0.0021 vol % epoxy, 24 vol % TEOS, and various amounts of F-silane. The bare stainless steel plates serve as blank sample. The increases in contact angles of water and oil occur at F-silane = 0.2 vol %. [Color figure can be viewed in the online issue, which is available at wileyonlinelibrary.com.]

RESULTS AND DISCUSSION

Thickness of Epoxy Films on Stainless Steel Plate

As the steel substrate has long-range surface roughness, it is difficult to locate a clear-cut film edge of the relatively thin films. Even if the film edge is distinct to the eye, the film thickness has to be determined by the difference in mean height between both sides of the film edge. Therefore, to measure the thickness of epoxy films on steel plate, a surface profilometer is used rather than AFM, because the former is able to scan a length of several millimeters. Surface height variation is revealed by profilometer as shown in Figure 2.

For bare stainless steel surface, the curve in Figure 2(A) gives an $Rq \sim 35$ nm, confirming that the shiny surface is nanoscopically smooth. For epoxy-coated steel surface, the curve in Figure 2(B) shows an enlarged height span; the left half of the curve corresponds to the surface profile of the steel plate, whereas the right one corresponds to that of the epoxy film. The average film thickness is calculated as the difference between the mean height of the left and right profiles. Both parts have similar *Rq*, but their mean heights differ by 80 nm, referred to as the thickness of epoxy film. The thicknesses of all the films on steel plates were measured in the same way.

The film precursor is mainly a solution of solvents except for the 24 vol % TEOS. To understand how the film thickness changes with the amount of added epoxy, a plot of film thickness, measured by the profilometer, is graphed against epoxy concentration. In spin coating, the deposited film is often reported to increase with the precursor concentration due to the increase in viscosity.[47,48] In Figure 3, a straight linear was used to merely show that the film grows in thickness in a certain manner with the epoxy content. However, the real correlation is expected to be more complex. To obtain a thin film no thicker than 150 nm, a 0.002 vol % was chosen between 0.001 and 0.01 vol %. The small amount of epoxy was found enough to help the precursor form an amphiphobic film on the substrate by spin coating. For films prepared at low epoxy volume percentage, the thickness falls in the range from 100 to 150 nm. In this study, the optimal condition is to expose the gloss of the steel substrate, thus, a 0.002 vol % is used in the subsequent experiments to obtain a coating thinner than 150 nm.

Contact Angle of Epoxy Films on Stainless Steel Plate

Contact angles of water and oil drops on bare and epoxy-/F-silane-coated stainless steel plates are plotted against F-silane volume percentage and shown in Figure 4. First, the freshly cleaned bare steel surface is high in surface energy and oleophilic with 0° oil contact angle, which is marked by the open triangle in the figure. The open circle denotes the water contact angle for bare steel surface. After the deposition of epoxy in the absence of F-silane, the coating surface exhibits similar

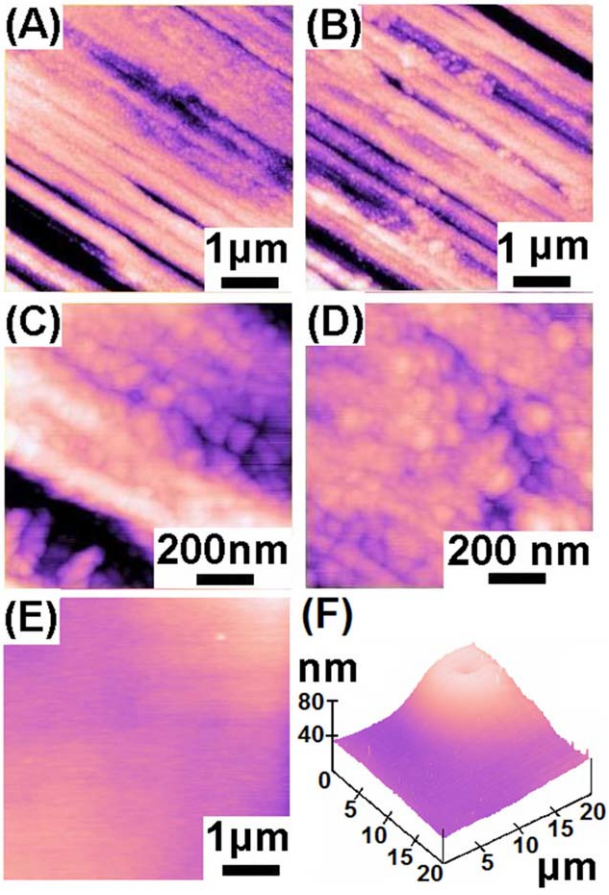

Figure 5. AFM images of bare (A) and epoxy-coated (B) stainless steel plates. The films were prepared from a solution containing 0.0021 vol % epoxy, 24 vol % TEOS, and no F-silane. Scan area = 5 μm × 5 μm. Height: from dark to bright = 60 nm. Enlarged AFM images of bare (C) and epoxy-coated (D) stainless steel plates. Scan area = 1 μm × 1 μm. Height: from dark to bright = 40 nm. E: Epoxy films coated on stainless steel plates with F-silane = 13 vol %. Scan area = 5 μm × 5 μm. Height: from dark to bright = 10 nm. F: Large perspective view of epoxy films coated on stainless steel plates with F-silane = 13 vol %. Scan area = 20 μm × 20 μm. Height: from dark to bright = 40 nm. [Color figure can be viewed in the online issue, which is available at wileyonlinelibrary.com.]

wettability, indicated by the little change in water and oil contact angles. However, once adding F-silane to the film precursor solution, both contact angles of water and oil for epoxy films increase to higher values by more than 40°. It is clearly shown that the increased amphiphobicity comes from the addition of F-silane, implying a distribution of the fluorinated side chains over the epoxy film surface.

It is also shown in Figure 4 that, as the F-silane volume percentage increases, the water contact angle gradually increases, whereas that of the oil decreases, indicating that adding more F-silane does not help to enhance the oleophobicity. The contact angles of amphiphobic coatings on silicon wafer also show similar behavior.[49] As surface wettability or amphiphobicity is usually dependent on surface structure or roughness as demonstrated by the Cassie model,[50–52] a morphological study of the film was resorted for explaining the phenomenon of oleophobicity descent encountered in our case.

Morphology of Epoxy Films on Stainless Steel Plate

In Figure 5, AFM images show the typical surface morphologies of bare [Figure 5(A,C)] and epoxy-coated [Figure 5(B,D)] stainless steel plates. In Figure 5(A,B), similar ridges and grooves are observed, stemming from the manufacturing process. These oriented ridges and grooves have a width <1 μm and height variation <10 nm and could be classified as the middle-range structures of the steel surface. As shown earlier in Figures 2 and 3, the long-range roughness and the film thickness are of the same magnitude, that is, the peak to valley distance of the surface profiles ranges from 50 to 150 nm, comparable with the thickness of films prepared at low epoxy volume percentage. Therefore, the micrometer-sized ridges and grooves revealed by AFM are contained in the millimeter-sized peaks and valleys revealed by profilometer. For such film thickness and substrate roughness, it is difficult to report any epoxy films from the substrate or to measure the film thickness by analyzing Figure 5(A,B).

In Figure 5(C,D), the further enlarged AFM images show fine granules over each ridge. The granules are all about 100 nm in diameter for both bare and coated surfaces. Similar to the ridges, the granules observed over the coated surface are not just epoxy but steel covered by epoxy. Referring to Series 2 in Table I, it was found that recipes in Rows 2 through 5 using low F-silane volume percentage gave a similar film morphology to that out of Row 1 without F-silane. Therefore, only the AFM images of recipe in Row 1 are shown. Based on the multiscale morphologies revealed by AFM and profilometer, it is speculated that the deposited epoxy is not only adsorbed onto the granular steel surface but also absorbed into the grooves due to the capillarity effect. As shown in Figure 5(E), all the steel surface features are seen hidden out by epoxy films at high F-silane volume percentage. The recipe is given in the last row of Series 2 in Table I. It used 13 vol % of F-silane and gave not only a thickened film but also small bumps as shown in Figure 5(F). The masking out of surface features and the emergence of bumps are believed to cause the decline of the oil contact angle as shown in Figure 4. It is then concluded that the film morphology traces out that of the steel substrate at low epoxy and F-silane volume percentage, but smoothes out gradually as the F-silane content in the precursor solution increases.

As shown in Figure 4, it is observed that both the bare steel and the epoxy-only coating give a water contact angle $\sim 70°$, indicating that the native surface roughness of the steel plate is not sufficient to reach hydrophobicity ($>90°$). It is then obvious that such hierarchical structures from long-range roughness to middle-sized ridges to nanogranules on steel surface are not specially designed to give optimal spacing, width, and height, as discussed in examples found in the cited references.

CONCLUSIONS

In this report, we show that the deposition of thin epoxy films onto stainless steel plate by spin coating can generate a surface oleophobicity that is boosted by the addition of a tiny amount of F-silane. Although the steel surface comprises hierarchical structures from wavy bundles of ridges to nanogranules, it is not specially designed to give optimal patterns when compared with those by carefully controlled deposition or etching. This work examines the common structures of steel surface made of current designs and suggests that with an improved rolling process, an optimal multiscale surface structure of stainless steel to render superamphiphobicity and durability for repetitive use can be achieved. Our study provides a formulated method of identifying the optimal amphiphobic coating thickness; which can be used to evaluate the efficiency of these coatings on self-cleaning products and to determine the most cost-effective coating quantity.

ACKNOWLEDGMENTS

This work received financial support from the National Science Council of Taiwan, Republic of China (NSC 93-2622-E-035-002-CC3) and Sakura, Taiwan. The authors thank Ms. Ya-Hui Chen at the Precision Instruments Service Center of Feng Chia University for AFM works.

REFERENCES

1. Liu, K.; Tian, Y.; Jiang, L. *Prog. Mater. Sci.* **2013**, *58*, 503.
2. Liu, K. S.; Jiang, L. *Nanoscale* **2011**, *3*, 825.
3. Koch, K.; Bhushan, B.; Ensikat, H. J.; Barthlott, W. *Philos. Trans. R. Soc. A: Math. Phys. Eng. Sci.* **2009**, *367*, 1673.
4. Zheng, Y. M.; Gao, X. F.; Jiang, L. *Soft Matter* **2007**, *3*, 178.
5. Gao, X. F.; Yan, X.; Yao, X.; Xu, L.; Zhang, K.; Zhang, J. H.; Yang, B.; Jiang, L. *Adv. Mater.* **2007**, *19*, 2213.
6. Feng, L.; Zhang, Y. A.; Xi, J. M.; Zhu, Y.; Wang, N.; Xia, F.; Jiang, L. *Langmuir* **2008**, *24*, 4114.
7. Zheng, Y. M.; Bai, H.; Huang, Z. B.; Tian, X. L.; Nie, F. Q.; Zhao, Y.; Zhai, J.; Jiang, L. *Nature* **2010**, *463*, 640.
8. Verho, T.; Bower, C.; Andrew, P.; Franssila, S.; Ikkala, O.; Ras, R. H. A. *Adv. Mater.* **2011**, *23*, 673.
9. Yao, X.; Gao, J.; Song, Y. L.; Jiang, L. *Adv. Funct. Mater.* **2011**, *21*, 4270.
10. Spagnol, V.; Cachet, H.; Baroux, B.; Sutter, E. *J. Phys. Chem. C* **2009**, *113*, 3793.

11. Kwon, Y. B.; Weon, B. M.; Won, K. H.; Je, J. H.; Hwu, Y.; Margaritondo, G. *Langmuir* **2009**, *25*, 1927.
12. Liu, M. J.; Wang, S. T.; Wei, Z. X.; Song, Y. L.; Jiang, L. *Adv. Mater.* **2009**, *21*, 665.
13. Joly, L.; Biben, T. *Soft Matter* **2009**, *5*, 2549.
14. Darmanin, T.; Nicolas, M.; Guittard, F. *Langmuir* **2008**, *24*, 9739.
15. Yang, Y. G.; Nakazawa, M.; Suzuki, M.; Shirai, H.; Hanabusa, K. *J. Mater. Chem.* **2007**, *17*, 2936.
16. Tuteja, A.; Choi, W.; Ma, M. L.; Mabry, J. M.; Mazzella, S. A.; Rutledge, G. C.; McKinley G. H.; Cohen, R. E. *Science* **2007**, *318*, 1618.
17. Cassie, A. B. D.; Baxter, S. *Nature* **1945**, *155*, 21.
18. Wenzel, R. N. *J. Phys. Colloid Chem.* **1949**, *53*, 1466.
19. Jung, Y. C.; Bhushan, B. *J. Microsc (Oxford)* **2008**, *229*, 127.
20. Wang, C. F.; Chiou, S. F.; Ko, F. H.; Chou, C. T.; Lin, H. C.; Huang, C. F.; Chang, F. C. *Macromol. Rapid Commun.* **2006**, *27*, 5.
21. Li, H. J.; Wang, X.; Song, Y. L.; Liu, Y.; Li, Q.; Jiang, L.; Zhu, D. B. *Angew. Chem. Int. Ed. Engl.* **2001**, *40*, 4.
22. Xie, Q.; Xu, J.; Feng, L.; Jiang, L.; Tang, W.; Luo, X.; Han, C. C. *Adv. Mater.* **2004**, *16*, 4.
23. Wang, S. W.; Feng, L.; Liu, H.; Sun, T.; Zhang, X.; Jiang L.; Zhu, D. B. *ChemPhysChem* **2005**, *6*, 4.
24. Tian, Y.; Liu, H.; Deng, Z. *Chem. Mater.* **2006**, *18*, 3.
25. Li, Y.; Li, C.; Cho, S. O.; Duan, G.; Cai, W. *Langmuir* **2007**, *23*, 6.
26. Shiu, J. Y.; Chen, P. L. *Adv. Funct. Mater.* **2007**, *17*, 7.
27. Shiu, J. Y.; Kuo, C. W.; Chen, P. L.; Mou, C. Y. *Chem. Mater.* **2004**, *16*, 4.
28. Senesi, G. S.; D'Aloia, E.; Gristina, R.; Favia, P.; d'Agostino, R. *Surf. Sci.* **2007**, *601*, 7.
29. Bernett, M. K.; Zisman, W. A. *J. Phys. Chem.* **1962**, *66*, 2.
30. Shafrin, E. G.; Zisman, W. A. *J. Phys. Chem.* **1960**, *64*, 6.
31. Sheen, Y. C.; Huang, Y. C.; Liao, C. S.; Chou, H. Y.; Chang, F. C. *J. Polym. Sci. Part B: Polym. Phys.* **2008**, *46*, 7.
32. Guo, M.; Ding, B.; Li, X.; Wang, X.; Yu, J.; Wang, M. *J. Phys. Chem. C* **2010**, *114*, 6.
33. Xiong, D.; Liu, G.; Zhang, J. H.; Duncan, S. *Chem. Mater.* **2011**, *23*, 11.
34. Frank, B. P.; Belfort, G. *Langmuir* **2001**, *17*, 8.
35. Lemal, D. M. *J. Org. Chem.* **2004**, *69*, 11.
36. Massoudi R.; King, A. D., Jr. *J. Phys. Chem.* **1975**, *79*, 4.
37. Schwinn, T.; Gaub, H. E. *Supramol. Sci.* **1994**, *1*, 6.
38. Li, X. M.; Reinhoudt, D.; Crego-Calama, M. *Chem. Soc. Rev.* **2007**, *36*, 1350.
39. Adolf, D.; Martin, J. E.; Wilcoxon, J. P. *Macromolecules* **1990**, *23*, 5.
40. Ferrer, M. L.; del Monte, F. *J. Phys. Chem. B* **2005**, *109*, 7.
41. Sivasankar, S.; Chu, S. *Nano Lett.* **2007**, *7*, 4.
42. Khayet, M.; Feng, C. Y.; Matsuura, T. *J. Membr. Sci.* **2003**, *213*, 22.
43. Yuan, W. L.; O'Rear, E. A.; Grady, B. P.; Glatzhofer, D. T. *Langmuir* **2002**, *18*, 9.
44. Hierlemann, A.; Campbell, J. K.; Baker, L. A.; Crooks, R. M.; Ricco, A. J. *J. Am. Chem. Soc.* **1998**, *120*, 2.
45. Nakajima, A.; Hashimoto, K.; Watanabe, T. *Langmuir* **2000**, *16*, 4.
46. Namai, Y.; Matsuoka, O. *J. Polym. Sci. Part B: Polym. Phys.* **2006**, *110*, 3.
47. Mohajerani, E.; Farajollahi, F.; Mahzoon, R.; Baghery, S. *J. Optoelectron Adv. Mater.* **2007**, *9*, 12.
48. Rengifo, H. R.; Chen, L.; Grigoras, C.; Ju, J.; Koberstein, J. T. *Langmuir* **2008**, *24*, 7450.
49. Mou, C. Y.; Yuan, W. L.; Shih, C. H. *Thin Solid Films* **2013**, *537*, 202.
50. Gao, L.; McCarthy, T. J. *Langmuir* **2006**, *22*, 2.
51. Marmur, A. *Langmuir* **2003**, *19*, 6.
52. Sun, M.; Luo, C.; Xu, L.; Ji, H.; Ouyang, Q.; Yu, D.; Chen, Y. *Langmuir* **2005**, *21*, 4.